Journal of Magnetic Resonance 205 (2010) 161–170

Contents lists available at ScienceDirect

Journal of Magnetic Resonance

journal homepage: www.elsevier.com/locate/jmr

Adapted RF pulse design for SAR reduction in parallel excitation with experimental verification at 9.4 T

Xiaoping Wu, Can Akgün, J. Thomas Vaughan, Peter Andersen, John Strupp, Kâmil Uğurbil, Pierre-François Van de Moortele *

Center for Magnetic Resonance Research, Department of Radiology, University of Minnesota Medical School, Minneapolis, MN, USA

ARTICLE INFO

Article history:
Received 19 November 2009
Revised 28 April 2010
Available online 5 May 2010

Keywords:
Parallel excitation
RF pulse design
Specific absorption rate
High magnetic field MRI
2D VERSE pulse

ABSTRACT

Parallel excitation holds strong promises to mitigate the impact of large transmit B_1 (B_1^+) distortion at very high magnetic field. Accelerated RF pulses, however, inherently tend to require larger values in RF peak power which may result in substantial increase in Specific Absorption Rate (SAR) in tissues, which is a constant concern for patient safety at very high field. In this study, we demonstrate adapted rate RF pulse design allowing for SAR reduction while preserving excitation target accuracy. Compared with other proposed implementations of adapted rate RF pulses, our approach is compatible with any k-space trajectories, does not require an analytical expression of the gradient waveform and can be used for large flip angle excitation. We demonstrate our method with numerical simulations based on electromagnetic modeling and we include an experimental verification of transmit pattern accuracy on an 8 transmit channel 9.4 T system.

1. Introduction

Recently, there has been increasing interest in using parallel excitation [1,2] to accelerate multidimensional spatially selective RF pulses [3,4]. This approach is especially promising to mitigate severe transmit (Tx) B_1 inhomogeneities observed at high magnetic field [5,6] where short T2 and T2* relaxation constants impose stronger limits on RF pulse duration [7–9]. However, using shorter RF pulses for a given flip angle intrinsically tends to increase RF magnitude, resulting in higher RF power and thus higher specific absorption rate (SAR) in tissue [10–12]. This is a serious concern at high magnetic field since larger RF power is needed to reach a given flip angle excitation at higher magnetic field [13].

Therefore, it is critical to develop accelerated RF pulse design methods capable of limiting or reducing SAR levels. Most approaches that have been proposed in this direction can be separated in two groups. The first group relies on a fixed gradient waveform which is unchanged through the RF pulse design. Here, SAR limitation is obtained by RF pulse (but not gradient waveform) manipulation, based on solving an optimization problem using explicit RF pulse regularization [7,14] or electrodynamic constraints [15,16] while maintaining excitation fidelity. In the second group of methods, the gradient waveform or excitation k-space trajectory is altered in order to reduce RF peak magnitude in RF pulses, thus reducing SAR. In the implementation proposed by Graesslin et al. [17] the traversal rate of a chosen k-space trajectory is adapted based on filtered FFTs of the desired excitation patterns. This implementation however assumes RF waveforms and resulting excitation patterns to be linked by a direct Fourier transform, which is only verified with small tip angles [4], so it would not provide optimal RF pulses for large tip angles [18]. Another implementation introduced by Xu et al. [19] relies on designing variable slew rate spiral gradients for reducing RF peaks based on initially calculated RF pulses. This method does not assume a Fourier transform relationship between RF pulses and resulting excitation patterns, and thus can be used with large tip angles. However, the corresponding formalism relies on an analytical representation of the initial gradient waveforms to calculate slew rate adjustments, thus it is restricted only to certain gradient waveforms. More recently, Lee et al. [20], referring to the initial concept that we previously introduced [21], proposed a general approach to achieve gradient alterations for SAR reduction in multidimensional and parallel transmit selective excitation by designing time optimal gradient waveforms with new gradient amplitude constraints calculated from peak RF limits. However, there was no *experimental* demonstration in this numerical simulation study. Furthermore, neither main field inhomogeneity nor gradient imperfections were considered, two components that require, when present, to be corrected for to preserve excitation accuracy in RF pulse design at high field [22]. Also, in this approach, final adapted RF pulses were designed with direct manipulation of original RF pulses rather than with RF

* Corresponding author. Address: Center for Magnetic Resonance Research, University of Minnesota Medical School, 2021 6th Street S.E., Minneapolis, MN 55455, USA. Fax: +1 612 626 2004.
E-mail address: pfvdm@cmrr.umn.edu (P.-F.).

1090-7807/$ - see front matter © 2010 Elsevier Inc. All rights reserved.
doi:10.1016/j.jmr.2010.04.018

recalculation based on final adapted gradient waveforms (it will be seen in the present work that this latter step can be necessary in some cases).

In the implementation that we have introduced [21], the gradient waveform modulation allowing for RF peak power reduction is calculated by adapting the gradient amplitude similarly to the variable-rate selective excitation, or VERSE, initially introduced by Conolly et al. for RF pulses with a single transmit channel [23]. Our method can provide optimal RF pulse for both small and large flip angle, can be used with any gradient waveform (it does not require an analytical description of the latter) and explicitly accounts for main field inhomogeneity and gradient imperfections. We have previously reported numeric simulations [21] and experimental verification [24] in the form of scientific conference abstracts. In this paper, we give a complete description of this approach, including a 3-step procedure for RF pulse design, which is compared against simply stretching RF pulse and gradient waveform in the temporal dimension. Our numerical simulations based on 2D RF pulses designed at 9.4 T for 8 Tx channels with a reduction factor of 4 ($R = 4$) indicate that substantial SAR reduction can be obtained with very limited increase in RF pulse duration. Our experimental results also demonstrate that with this approach RF excitation pattern accuracy is preserved.

2. Theory

2.1. RF power dissipation

The RF energy deposited into tissues during RF pulsing typically increases with the static magnetic field strength [13,25–27]. In parallel excitation, the average SAR produced in a voxel at location $\mathbf{r}$ by an RF pulse of duration T with N Tx channels can be expressed as [28]:

$$\mathrm{SAR}(\mathbf{r}) = \frac{\sigma(\mathbf{r})}{2\rho(\mathbf{r})T}\int_0^T \left|\sum_{n=1}^{N}\mathbf{E}_{0,n}(\mathbf{r})b_{1,n}(t)\right|^2 \mathrm{d}t \tag{1}$$

where σ and ρ represent the conductivity and mass density of the scanned object, respectively. $\mathbf{E}_{0,n}$ is the complex-valued E field of the nth Tx channel driven by a unit current for a given load, and $b_{1,n}(t)$ is the complex-valued RF pulse applied through the nth Tx channel.

2.2. Adapted-rate parallel excitation

In this work we extend to multiple Tx channels and 2D RF pulse the VERSE technique introduced for 1D slice selective RF pulse with a single Tx channel by Conolly et al. [23]. The VERSE method is based on the variable rate principle stating that, ignoring relaxation and diffusion terms, changes in magnitude and duration of a magnetic field will not induce a change in the rotation of magnetization if the field surface (field strength × duration time) remains unchanged. Therefore, when an RF pulse is applied together with spatial encoding gradients (e.g., slice excitation), it is possible to simultaneously alter RF pulse shape *and* gradient waveform while retaining a same flip angle for on-resonance isochromats. On the other hand, as shown in Eq. (1), SAR is proportional to the time integral of the *squared* magnitude of the electric field induced by an RF pulse, indicating that RF pulses with lower peak values may give rise to less SAR for a given flip angle and pulse duration. Thus, high RF peaks can be suppressed with gradient waveforms modified accordingly to reduce SAR for a target flip angle. This simultaneous manipulation can be realized by introducing a time control function. Let $B_1(\mathbf{r}, t)$ and $\mathbf{G}(t)$ respectively denote the Tx B_1 field and the multidimensional gradient waveform to be adapted. The adapted Tx B_1 field $B_1^{\mathrm{ad}}(\mathbf{r}, t)$ and gradient waveform $\mathbf{G}^{\mathrm{ad}}(t)$ for the same flip angle can be given by:

$$B_1^{\mathrm{ad}}(\mathbf{r}, t) = B_1(\mathbf{r}, \tau(t))\dot{\tau}(t) \tag{2}$$

$$\mathbf{G}^{\mathrm{ad}}(t) = \mathbf{G}(\tau(t))\dot{\tau}(t) \tag{3}$$

Here the time control function $\tau(t)$ has the same units of time and satisfies $\tau(0) = 0$ and $\tau(T^{\mathrm{ad}}) = T$ (T and T^{ad} are the *original* and *adapted* pulse durations, respectively). The dot denotes the time derivative. The manipulations defined in Eqs. (2) and (3) do not change the surface of the net magnetic field (i.e., the time integral of the sum of RF and gradient related magnetic fields) and therefore retain the flip angle. Although the manipulation in Eq. (2) is applied on the total Tx B_1 field, it can be directly translated to multiple Tx channels. In parallel excitation, since the relationship between total Tx B_1 field and RF pulses is linear, the desired manipulation of the total Tx B_1 field can be implemented by applying the same operation on individual RF pulses. Therefore, Eq. (2) can be replaced by a series of equations

$$b_{1,n}^{\mathrm{ad}}(t) = b_{1,n}(\tau(t))\dot{\tau}(t) \tag{4}$$

where $n = 1, 2, \ldots, N$ (N is the number of Tx channels), $b_{1,n}^{\mathrm{ad}}(t)$ and $b_{1,n}(t)$ are the adapted and original RF pulses, respectively.

2.2.1. Design of time control function

A key task in adapted-rate parallel excitation is to find a time control function that can limit the peaks of the resulting RF pulses. One possible way to design such a time control function is to attenuate and elongate the original RF pulse and gradient waveform whenever the corresponding level of SAR is too high. When a single Tx channel is used, SAR is directly proportional to the square of the RF amplitude $|b_1|$, thus it is possible to use a simple $|b_1|$ threshold above which RF output is considered too high. If we further assume that RF and gradient amplitudes are never to be increased, which is equivalent to say that $\dot{\tau}(t)$ can never be greater than unity, the time control function can be defined as:

$$\dot{\tau}(t) = \begin{cases} \frac{a}{|b_1(t)|} & \text{if } |b_1(t)| > a \\ 1 & \text{otherwise} \end{cases} \tag{5}$$

where a is a threshold which can in principle take any value in the range $(0, |b_1(t)|_{\max})$ with $|b_1(t)|_{\max}$ being the maximum value of the RF pulse shape $|b_1(t)|$. Naturally, lowering the threshold a yields RF pulse peaks that are further suppressed with lower SAR levels, but at the cost of longer RF pulse duration.

In the case of multiple Tx channels that are each playing a different RF pulse shape, SAR for each time point cannot anymore be expressed as directly proportional to a squared $|b_1|$ quantity. In theory, the only way to express SAR(t) is then to compute the net electric field produced by each complex $b_{1,n}(t)$ combination in Eq. (1), but this would not be practical to calculate SAR reduction on-the-fly during an in vivo MR experiment because electric fields cannot be mapped with current MRI techniques. One possibility is to utilize electromagnetic models, but these highly depend on specific RF coil designs and on anatomical variations between subjects, so that such implementation would lack generality. Fortunately, we consistently observed in our numerical simulations, obtained with different RF coil designs, different excitation targets and different anatomical targets, a high correlation between the sum of the RF magnitudes (RFSOM) through all Tx channels and the corresponding spatially averaged total E field. We further verified that, in multi Tx RF pulse design, RFSOM can be reliably used to determine a threshold a above which RF peaks are considered too high, with the time control function now written as:

$$\dot{\tau}(t) = \begin{cases} \frac{a}{\mathrm{RFSOM}(t)} & \text{if RFSOM}(t) > a \\ 1 & \text{otherwise} \end{cases} \quad (6)$$

Here the threshold a can take any value between 0 and the maximum of RFSOM(t).

As will be shown, the time control function given by Eq. (6) along with the threshold a, which can for example be defined as the temporal average of RFSOM, can be used to design adapted RF pulses with reduced RF power in small tip angle RF excitation (e.g., nominal FA = 20°). However, in case of large tip angle excitation (e.g., nominal FA = 90°), this formulation may result in adapted RF peak power that still exceeds the limits of the MR system, and thus is not applicable. Although the adapted RF peak power can be further reduced by decreasing the threshold a below the time average of RFSOM, it would not anymore reflect the actual RF power limit to be addressed and could yield overly conservative solutions with unnecessarily long RF pulses. Therefore, a different time control function explicitly utilizing the individual RF pulse shapes (instead of RFSOM) of the original pulses can be considered for large tip angle pulse design, given by:

$$\dot{\tau}(t) = \begin{cases} \frac{a}{\mathrm{bMAX}(t)} & \text{if bMAX}(t) > a \\ 1 & \text{otherwise} \end{cases} \quad (7)$$

where $\mathrm{bMAX}(t) = \max_{(n=1,2,\ldots,N)}\{|b_{1,n}(t)|\}$ represents the maximum RF magnitude among the eight original pulses at each time point, and the threshold a now specifies the maximum allowed RF magnitude in the resulting adapted pulses.

2.2.2. Pulse design

We propose a 3-step approach to designing adapted-rate parallel excitation RF pulses, demonstrated here with spiral gradient trajectories (spiral trajectories are most often chosen in parallel excitation given their high time k-space coverage efficiency). First, original parallel excitation RF pulses are calculated using slew rate limited gradient waveforms (for experimental results ΔB_0 maps are measured and included in RF pulse calculation). Second, a RFSOM threshold is determined and gradient waveforms are modified using a time control function defined by the originally calculated pulses (Eqs. (3) and (6)). Last, in order to retain excitation fidelity, the final adapted rate RF pulses are calculated based on the new adapted gradients, rather than from direct manipulation of the original RF pulses with the time control function used for the gradient waveform (Eq. (4)). A critical reason for this choice is to address practical issues, e.g., B_0 inhomogeneities and gradient imperfections, when designing adapted rate multi Tx RF pulses, especially at high field. Indeed, it is well known that adapted rate RF pulses are inherently sensitive to off resonance induced distortions [23]. Also, it has been shown that drastic degradation of parallel excitation accuracy may result from residual gradient waveform errors [22]. In our implementation, these issues can be readily addressed by explicitly including ΔB_0 as well as gradient measurements during the final adapted RF pulse calculation. Another reason for RF recalculation is that the gradient waveforms obtained right after Eq. (3) may still require minor alterations to be actually usable by the scanner (e.g., interpolation and smoothing in order to never exceed maximum slew rate), resulting in deviations of the adapted k-space trajectory from the original one. This deviation needs to be compensated for by RF redesign.

3. Materials and methods

In this study, an elliptical eight-channel transceiver array built for 9.4 T [29] was considered. All computations, except for electromagnetic field simulations, were performed in MATLAB (MathWorks, Inc., Natick, MA) on a Pentium Linux workstation with 6 GB of RAM.

3.1. Pulse calculation

All parallel excitation RF pulses were calculated using the non-iterative linear class large tip angle (LCLTA) pulse design method [30]. With this method, RF pulses can be obtained by solving a Tikhonov regularization problem, $\min_{\boldsymbol{b}}(||\boldsymbol{Ab} - \boldsymbol{\theta}||^2 + \lambda||\boldsymbol{b}||^2)$. Here matrix $\boldsymbol{A}$ involves excitation k-space trajectory and B_1^+ maps, vector $\boldsymbol{b}$ contains individual complex RF pulse shapes, vector $\boldsymbol{\theta}$ represents the desired flip angle distribution, and λ is the regularization parameter. In this study, all RF pulses were designed using spiral trajectories corresponding to a reduction factor of 4 in k-space. The regularization parameter, λ, was determined using the L-curve criterion [9,30]. In all pulse designs a region of interest (ROI) was defined to only include voxels located inside tissues (simulation) or phantom (experiment).

3.2. Numerical simulations

2D RF pulse design and corresponding 3D SAR computations were obtained at 9.4 T based on electromagnetic simulations (Fig. 1) calculated with the XFDTD software (version 6.3, Remcom Inc., PA, USA) for the eight-channel coil [31] loaded with a human head model provided with the XFDTD software ($2 \times 2 \times 2.5$ mm^3 resolution).

Slew rate limited gradient waveforms for a 2D spiral k-space trajectory [32] were originally designed (Fig. 2) for $R = 4$ (2.8 ms in pulse duration), assuming maximum slew rate of 166 T/m/s. The fully sampled k-space corresponded to a field of excitation

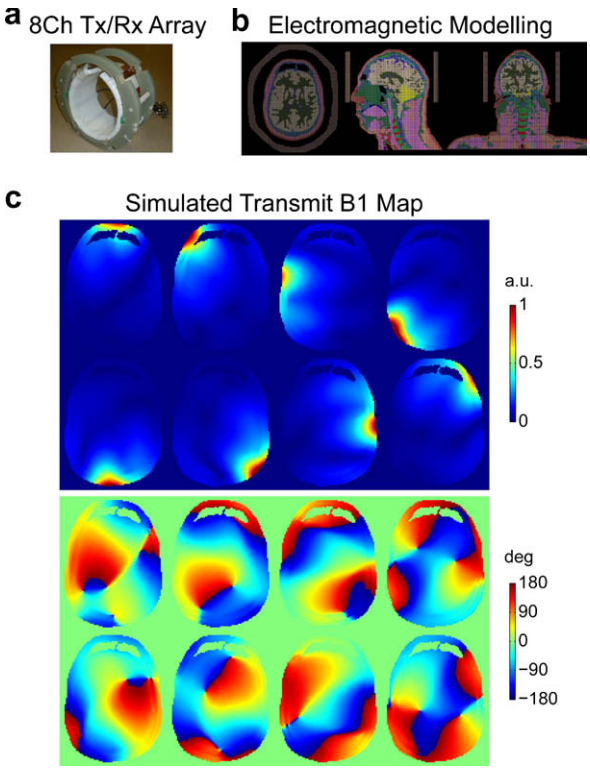

Fig. 1. XFDTD simulations at 9.4 T. (a) Picture of the elliptical eight-channel transceiver array considered in this study. (b) Axial (left), sagittal (middle) and coronal (right) views of the 3D FDTD model for the array in (a), loaded with a human head model. (c) Transmit B_1 magnitude (top panel) and phase (bottom panel) maps of individual channels of the array.

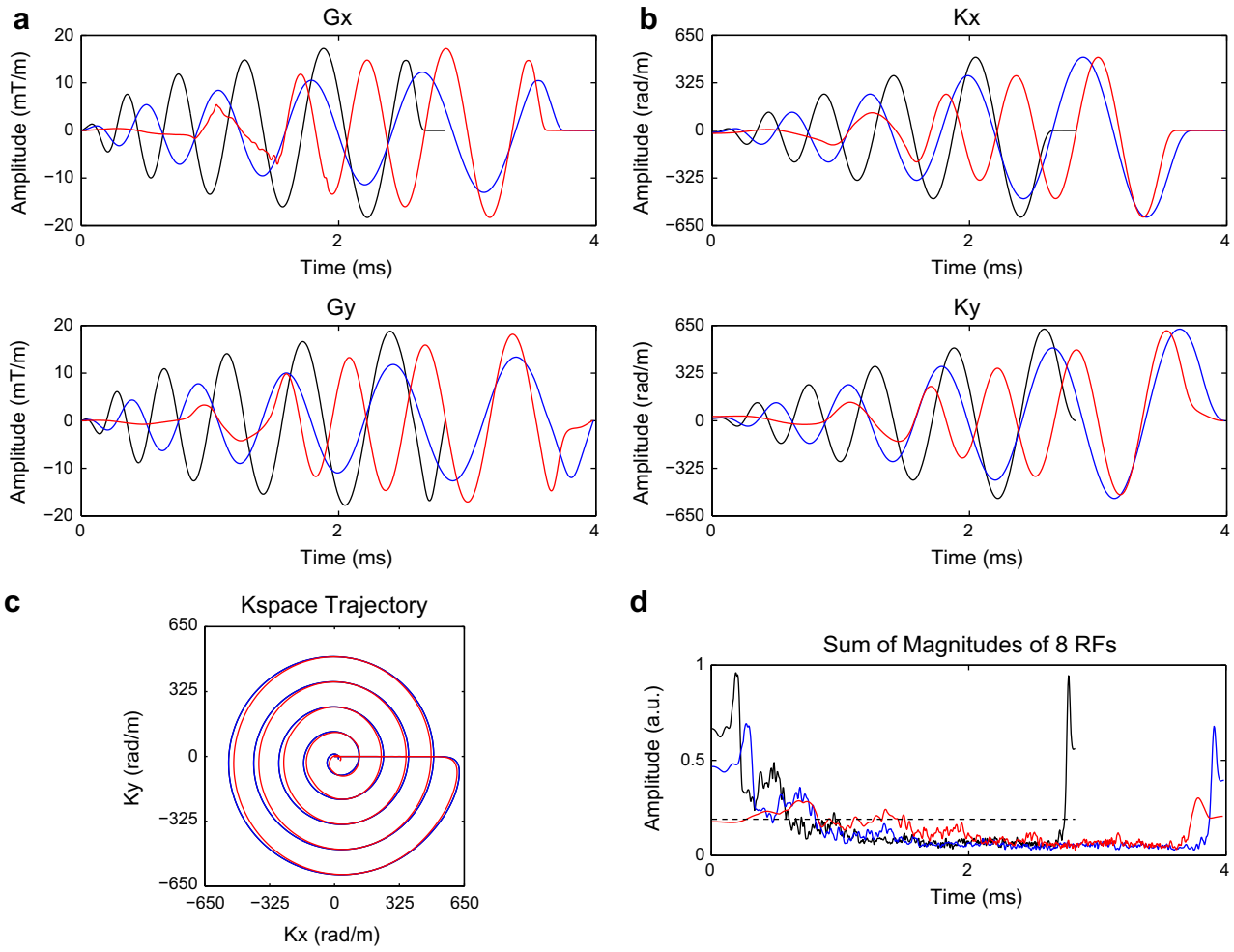

Fig. 2. Example of original (black), stretched (blue) and adapted (red) 2D parallel transmit RF pulse design based on simulations. (a) G_x and G_y waveforms. (b) Corresponding k_x and k_y waveforms. (c) k_x vs. k_y. Note that the stretched trajectory was identical to the original one and that only subtle deviations occur between adapted and original trajectories. (d) Sum of magnitude (RFSOM) of the eight RF pulses. The time average of the original RFSOM was used as the threshold (dashed line) in adapted pulse design. RF pulses with $R = 4$ were calculated for a large ellipse excitation target (Fig. 3a, top) using simulated transmit B_1 maps shown in Fig. 1. Note how the adaptive slowdown of k-space traversals effectively suppressed original large RF peaks. (For interpretation of the references to color in this figure legend, the reader is referred to the web version of this article.)

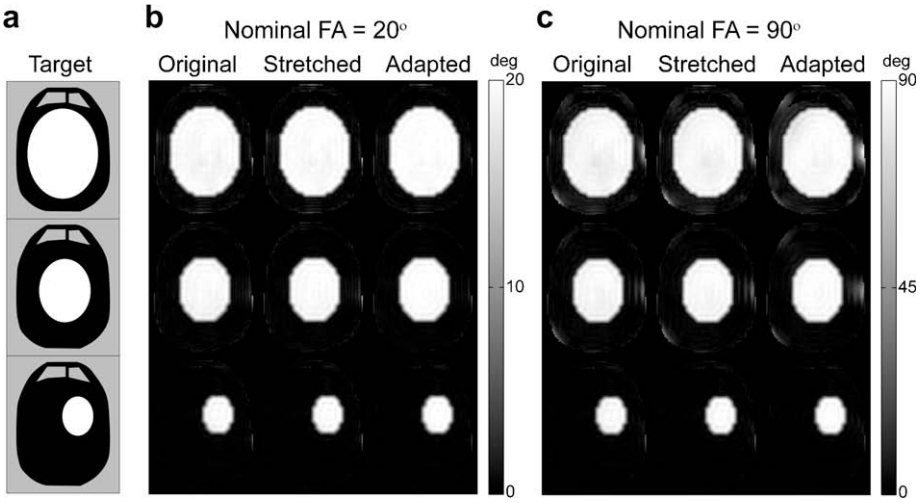

Fig. 3. Comparison of simulated excitation patterns of original, stretched and adapted parallel transmit RF pulses. (a) Three excitation targets. White color represents the nominal excitation flip angle (FA) (either 20° or 90°), black color indicates 0° FA, and gray color shows spin-free regions excluded in pulse design. (b and c) FA maps for a nominal FA of 20° (b) and 90° (c). Note excitation accuracy obtained with adapted RF pulses was comparable to that obtained with original and stretched RF pulses.

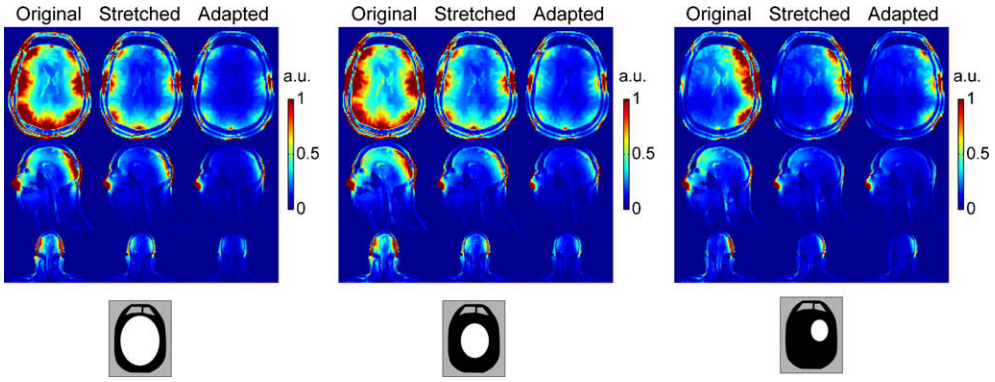

Fig. 4. Comparison of 3D SAR distributions between original, stretched and adapted parallel transmit RF pulse design. Three orthogonal views (from top to bottom: axial, sagittal and coronal) of SAR distributions are shown for three targets (shown at the bottom). Identical SAR patterns were observed for both 20° and 90° pulse design. Note that adapted RF pulses effectively reduced SAR as compared to original and stretched pulses. The FOV used for display was adjusted to the spatial extent of tissue present in each of the three views.

(FOX) of 20×20 cm^2 with a spatial resolution of 5 mm. Three excitation targets in an axial slice of the head (Fig. 3a) were considered: a large ellipse covering brain tissues, a centered intermediate ellipse, and an off centered small ellipse. In all displays of target patterns, white color represents the nominal excitation flip angle (20° or 90°), black color indicates 0° flip angle, and gray color shows spin-free regions excluded in pulse design. All patterns were defined on a 40×40 matrix in a FOX of 20×20 cm^2 centered on the gradient isocenter.

For each target, RF pulses were designed for both small (20°) and large (90°) nominal flip angles. For a given nominal flip angle, RF pulses were initially calculated using the originally designed gradient waveforms. The temporal average of RFSOM of these original RF pulses was used as the threshold value (parameter a in Eq. (6)) in gradient manipulations since it was found to provide a good balance between SAR reduction and pulse elongation. The resulting adapted gradient waveforms were then used to calculate the adapted RF pulses. Note that the modified gradient waveforms were re-sampled at a uniform sampling rate of 4 μs per dwell time to match format requirement on the scanner and were smoothed to not exceed the maximum slew rate before final RF calculations. For comparison, RF pulses were also designed using gradient waveforms that were simply stretched to reach the same duration as the adapted pulses by uniformly slowing down the original k-space traversal. The time control function used for this stretching manipulation was defined by the ratio of the pulse durations *before* and *after* adaptation, i.e., $\dot{\tau}(t) = T/T^{ad} < 1$. To evaluate excitation pattern fidelity, the resulting flip angle distributions (Fig. 3) defined on a finer 100×100 grid with 2-mm resolutions were obtained for the original, stretched and adapted RF pulses by performing Bloch simulations. Both pulse design and Bloch simulation assumed no B_0 inhomogeneity.

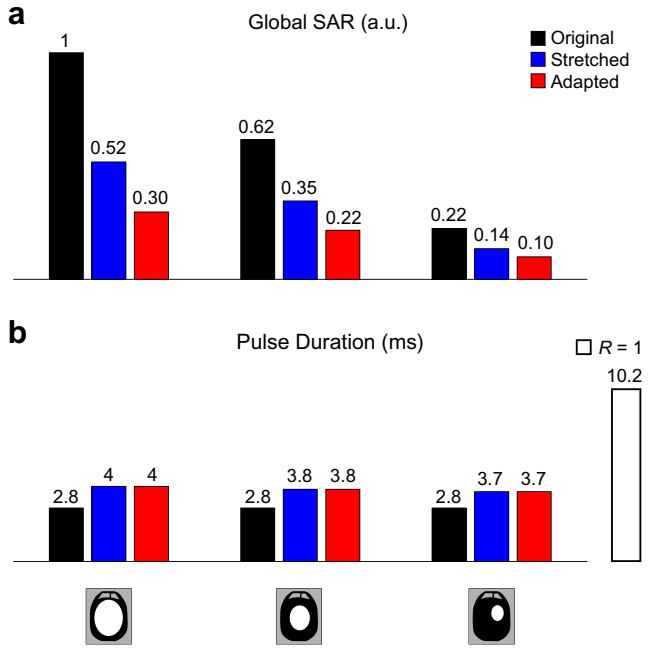

Fig. 5. Comparison of global SAR values (a) and of pulse durations (b) between original (black), stretched (blue) and adapted (red) parallel transmit RF pulse design. Global SAR values were calculated by summing up 3D SAR quantities within the human head, neck and shoulders as shown in Fig. 4. The pulse duration for full k-space sampling without reduction (i.e., $R = 1$) is also shown in white for comparison. Note that SAR was effectively decreased using adapted rate k-space trajectories for pulse design at the cost of a slight increase in pulse duration. (For interpretation of the references to color in this figure legend, the reader is referred to the web version of this article.)

3D SAR distributions generated by original, stretched and adapted RF pulses were computed over a volume that included the entire head and neck as well as the upper part of chest and shoulders ($52 \times 30 \times 30$ cm^3, $260 \times 150 \times 120$ FDTD cells). SAR value for individual cells and subsequent masking were determined as follows. SAR was first calculated for each of the 12 edges of a cell based on simulated E fields and using Eq. (1) (the FDTD gridding defines E fields and tissue properties on the edges of cells). The average of these 12 SAR numbers was then assigned to the cell.

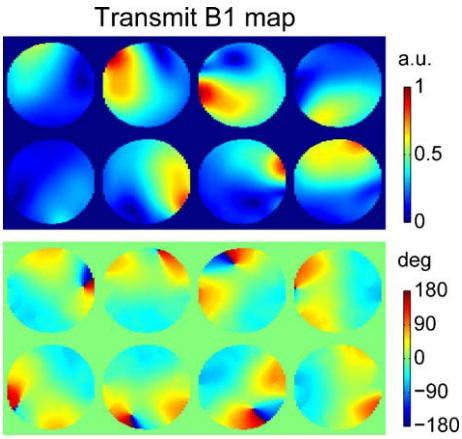

Fig. 6. Measured absolute magnitude (top panel) and relative phase (bottom panel) transmit B_1 maps of the 8 channel RF coil loaded with a spherical water phantom.

SAR maps were further masked in order to only retain valid cells, defined as having their 12 edges with nonzero conductivity and mass density. Global SAR was calculated by summing SAR values of all valid cells in the entire volume.

3.3. Experimental verification

Experiments were performed on a 9.4 T, 65-cm inner diameter bore human scanner (Magnex, UK), equipped with a head gradient coil capable of maximum gradient strength of 50 mT/m and slew rate of 166 T/m/s, interfaced to a VnmrJ/DirectDrive console (Varian, USA) that includes 16 independent Tx channels and 32 receive (Rx) channels. Eight Tx and eight Rx channels were used in this study, each Tx channel being powered with a 500 W RF amplifier (CPC, Brentwood, NY, USA). MR signals were acquired from a 16-cm-diameter spherical saline phantom (NaCl 99 mM) doped with copper sulfate (T1 $\sim$ 200 ms).

The eight complex B_1^+ maps of the RF coil were estimated by combining eight *relative* B_1^+ maps (magnitude and phase) and one *absolute* magnitude B_1^+ map. The relative maps were derived from eight gradient echo (GE) images collected at low flip angles with only one channel transmitting at a time, whereas the absolute magnitude map was obtained at high flip angles with all channels transmitting together using the actual flip angle technique (AFI) [33]. The eight GE images were acquired with TR/TE = 200/4 ms, slice thickness = 5 mm, FOV/matrix = 18 $\times$ 18 cm^2/128 $\times$ 64, and flip angles <4° around the center of the slice. The AFI was obtained with TR1/TR2/TE = 28/140/4.6 ms, slab thickness = 25 mm, and FOV/matrix = 18 $\times$ 18 $\times$ 7.5 cm^3/128 $\times$ 64 $\times$ 15. The total acquisition time of B_1^+ estimation for the eight channels was 4 min 24 s. Fig. 6 displays the eight measured transmit B_1 maps.

Eight product $\rho \times |B_1^-|$ maps of individual channels were also obtained, where ρ is proton density (constant in our homogeneous phantom) and $|B_1^-|$ is the receive B_1 sensitivity. These maps were estimated from GE images, acquired with the same set of RF phases and magnitudes as in AFI based B_1^+ mapping, and normalized with the sine of actual flip angle map. In addition, a ΔB_0 map (Fig. 9a) was measured using two GE images acquired at different echo times (TE1/TE2 = 8/9 ms) and was incorporated into RF pulse design to minimize off-resonance effects [7–9]. Note that B_1^+ shim [34,35] was performed prior to AFI and ΔB_0 mapping to reduce substantial B_1^+ destructive interferences between channels [36] observed when using the initial random B_1^+ phase of each RF channel observed after booting the multi Tx channel console.

Initial slew rate limited gradient waveforms were designed for maximum slew rate = 166 T/m/s and R = 4 (Fig. 7). The desired flip angle pattern was an off centered circle in an axial slice of the phantom, defined on a FOX of 18 $\times$ 18 cm^2 with a 5-mm resolution. This circle target was smoothed with a Gaussian filter to reduce the ringing artifacts in resulting excitation patterns. The peak values of

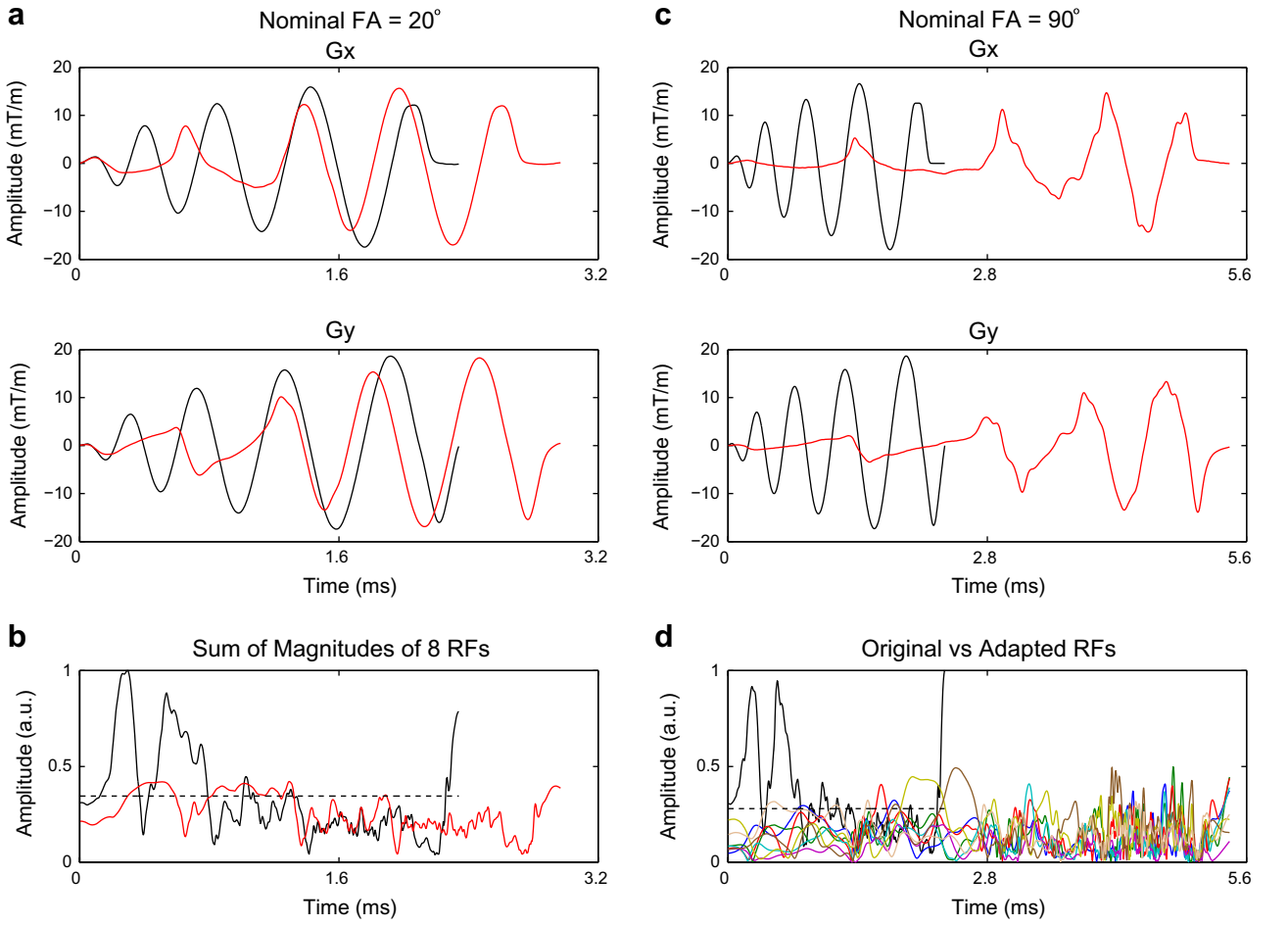

Fig. 7. Experimental RF pulse design for small (a and b) and large (c and d) tip angles. (a) Measured original (black) and adapted (red) gradient waveforms. (b) Sum of magnitudes of eight RF pulses (RFSOM) calculated with gradients in (a). The time average of RFSOM of original RF pulses designed with theoretical gradients was used as the threshold (dashed line) in adapted pulse design. (c) Theoretical original (black) and measured adapted (red) gradient waveforms. (d) RFSOM of originally calculated RF pulses divided by 8 (black) vs. 8 individual magnitudes of adapted RF pulses (shown in colors) calculated with measured gradients in (c). The threshold (dashed line) was determined in an ad hoc way based on the maximum available RF power. All RF pulses were designed for R = 4 in k-space and for a target as in Fig. 8a. (For interpretation of the references to color in this figure legend, the reader is referred to the web version of this article.)

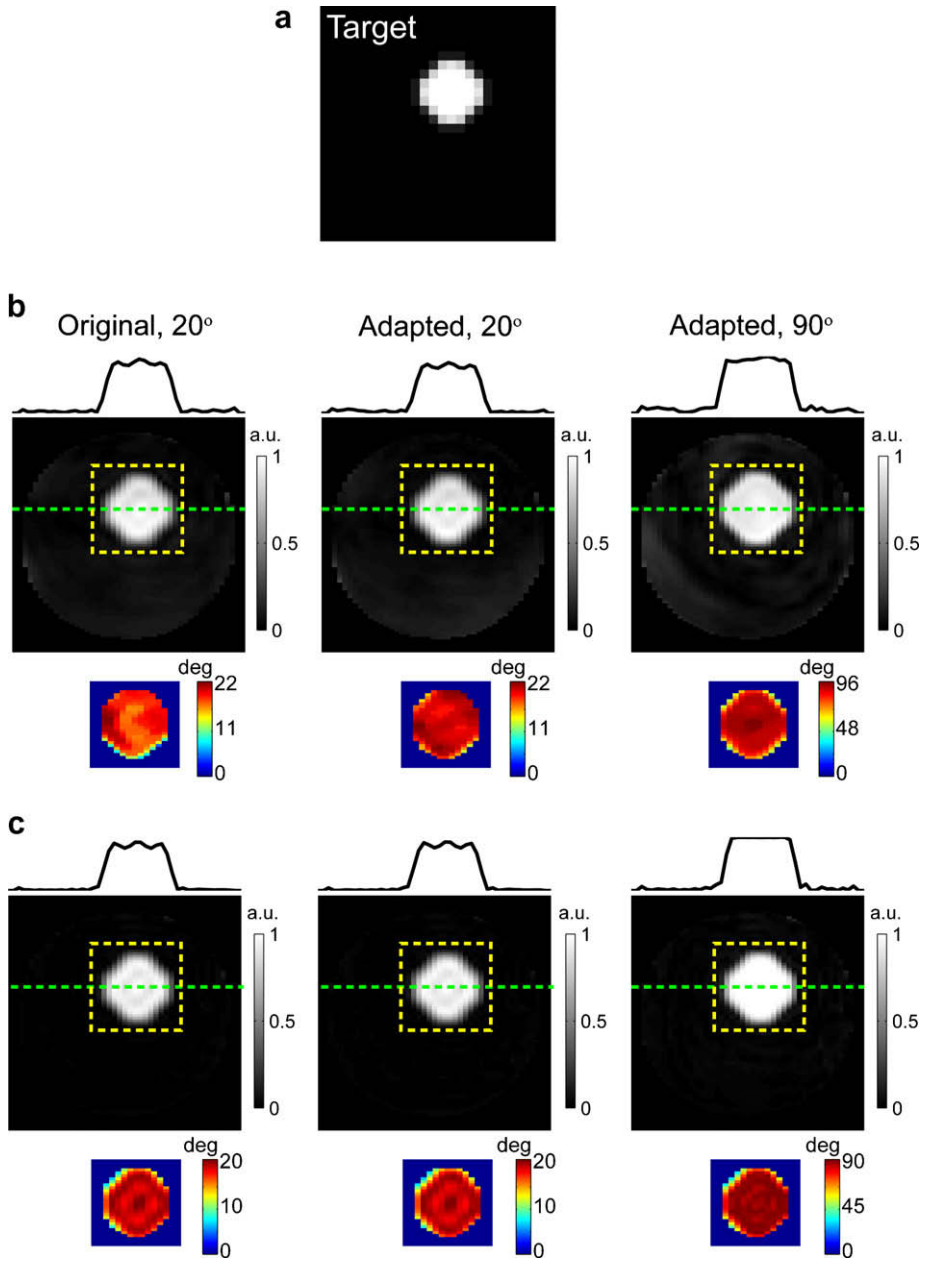

Fig. 8. Excitation pattern accuracy with adapted parallel transmit RF pulses. (a) Off centered circle flip angle target smoothed with a Gaussian filter, whose peak was scaled to 20° and 90° respectively for pulse design. (b) Experimental excitation patterns for original small (left), adapted small (middle) and adapted large (right) tip angle RF pulses as in Fig. 7. Excitation patterns were imaged with a modified 3D GE sequence and normalized for receive B_1 in order to mainly retain image intensity variations due to transmit B_1. Plots above images display intensity profiles along the green dashed line. Colored maps below images show masked flip angle distributions within the target circle. (c) Corresponding results obtained with Bloch simulations based on the same acquisition parameters. Note the satisfactory performance of adapted RF pulses for both small and large tip angles. (For interpretation of the references to color in this figure legend, the reader is referred to the web version of this article.)

the target were scaled to small (20°) and large (90°) nominal flip angles for RF pulse design.

For small tip angle RF excitation (nominal FA = 20°), adapted RF pulses with reduced RF power were designed as in the simulation study with the time control function given by Eq. (6) and with the threshold set to the temporal average of RFSOM. Experimental demonstration of large flip angle (nominal FA = 90°) *without* adaptation was not possible because the required RF peak power exceeded the maximum available RF power on our system, thus only *adapted* large flip angle data were acquired. In order to effectively consider the RF power limit of our system, adapted RF pulses of FA = 90° were calculated using the time control function defined in Eq. (7). Note that the threshold a was based on 90% of the maximum output RF power on each channel in order to reduce excitation errors due to RF amplifier nonlinearities that were observed when using 100% of the maximum RF power. Except for the different criteria described above to determine the time control function, all other components of RF pulse design were identical for small and large flip angles.

All RF pulses were calculated with actual *measured* gradient waveforms to minimize degradations of excitation patterns due to substantial gradient errors on our system despite of active eddy current compensation [22]. Actual G_x and G_y were measured in additional sessions using the method of Duyn et al. [37] which extracts k-space trajectories based on phase differences between two respective FID signals obtained with the test gradient turned on

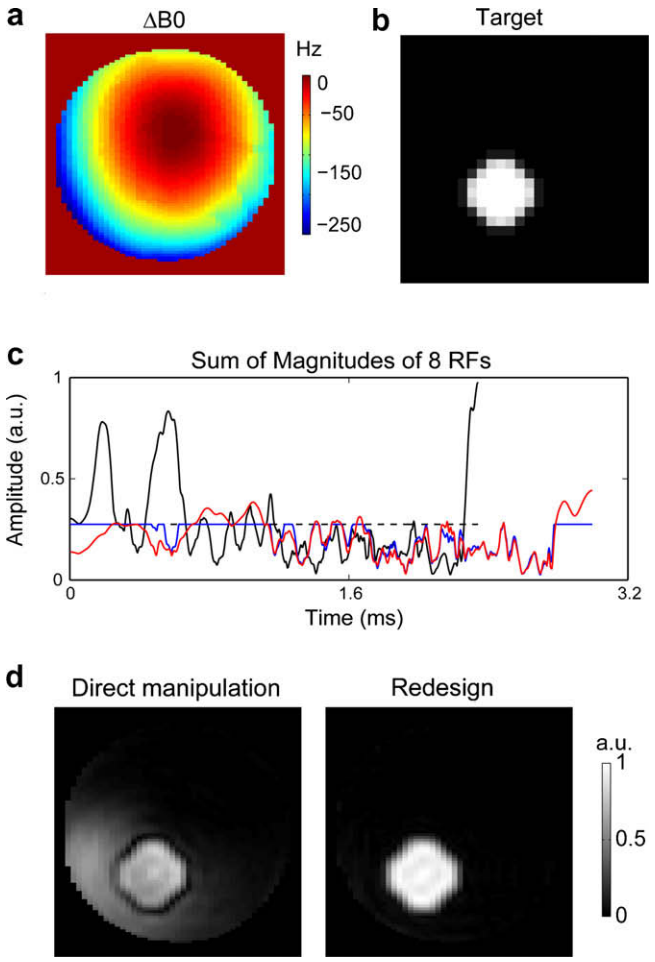

Fig. 9. Critical impact of the third step in the proposed RF pulse design. (a) Measured ΔB_0 map. (b) Off centered and filtered circle flip angle target (nominal flip angle = 20°). (c) Sum of magnitudes of eight adapted RF pulses (RFSOM) calculated by manipulation of original pulses using Eq. (4) (blue) vs. by RF redesign with ΔB_0 correction (red). The time average of original RFSOM (black) was used as the threshold (dashed line). (d) The resulting excitation patterns from Bloch simulations using the two pulse calculation schemes. Note that significant excitation errors mainly due to off-resonance effects occurred when manipulating original pulses (left) and were effectively removed by redesigning pulses (right). (For interpretation of the references to color in this figure legend, the reader is referred to the web version of this article.)

and off from a particular slice perpendicular to the gradient axis of interest. Note that in adapted RF pulse design, gradient measurements were only needed in the last step when final adapted pulses were calculated.

Excitation patterns of calculated RF pulses were imaged using a 3D GE pulse sequence where accelerated 2D selective excitations had been included. These 3D images were acquired with FOV/matrix = $18 \times 18 \times 15$ cm^3/$128 \times 64 \times 30$, TR/TE = 150/4 ms for small (20°) and TR/TE = 600/5.5 ms for large (90°) flip angles. The 2D views of the slice of interest were extracted from the 3D datasets and were normalized with the sum of magnitudes of the eight estimated $\rho \times |B_1^-|$ maps to mainly retain intensity variations due to RF excitation. Residual relaxation effects in final images were negligible in this homogeneous phantom. Flip angle distributions within the target circle were also mapped using AFI with TR1/TR2 = 28/140 ms and FOV/matrix = $18 \times 18 \times 15$ cm^3/$128 \times 64 \times 30$ for both small and large tip angle RF excitations. In addition, excitation results were computed based on Bloch simulations, ignoring relaxation and diffusion terms. In all simulations, we used the measured B_1^+ and ΔB_0 maps and defined the excitation pattern on an 18×18 cm^2 FOX with a 128×64 matrix, to match as closely as possible the experimental conditions.

In order to demonstrate that final adapted RF pulses need to be redesigned to achieve satisfactory excitation fidelity (third RF pulse design step), we performed additional simulations (based on experimentally measured B_1^+ and ΔB_0 maps) to compare the final adapted RF pulses with RF pulses only obtained by direct manipulation of the original pulses (i.e., using Eq. (4)). Here, no gradient smoothing or gradient measurement was considered in order to demonstrate that not correcting for B_0 inhomogeneity alone is sufficient to substantially degrade excitation accuracy. The excitation target in this case was a smoothed circle positioned in a location where large ΔB_0 had been measured in the phantom (Fig. 9b). Adapted RF pulses were designed for small tip angles (20°) with the time control function designed with the RFSOM. Corresponding Bloch simulations were conducted using the two types of adapted RF pulses to compare the resulting excitation patterns.

4. Results

In Fig. 2 are shown the original, stretched and adapted gradient waveforms and k-space trajectories as well as the corresponding RFSOM of RF pulses obtained in the simulation study when a large elliptical shape (Fig. 3a, top) was used as the target pattern. As can be seen in Fig. 2, adapting the gradient waveforms for RF pulse calculation was very effective in suppressing RF peaks (as defined by RFSOM) exceeding a defined threshold in the originally calculated RF pulses. Moreover, a direct comparison of RFSOM in Fig. 2d indicates that RF peak suppression was significantly more efficient with adapted pulses than with pulses simply stretched to the same final RF pulse duration. As expected, in adapted RF pulses strong k-space traversal slowdowns occurred to provide high temporal sampling density in the k-space when strong high RF peaks were observed in the initial RF pulses (Fig. 2b). One can notice that the adapted k-space trajectory (ignoring traversal speed) was marginally altered from the original one (Fig. 2c) due to further manipulations imposed on adapted gradients (i.e., interpolation and smoothing). Consequently, the SOM of the resulting adapted RF pulses violated the threshold at some places (Fig. 2d). Importantly, excitation patterns obtained from Bloch simulations, with different excitation targets and with different nominal flip angles (Fig. 3), showed that the excitation fidelity obtained with adapted RF pulses was comparable to that obtained with original and stretched RF pulses. For a given target, the difference between the normalized mean root squared errors calculated for the original, stretched and adapted RF pulses was up to 1.6% for small flip angle excitation and up to 2.6% for large flip angle excitation.

3D SAR maps were calculated in the whole volume using original, stretched and adapted RF pulses. Axial, sagittal and coronal views extracted from those 3D maps are shown in Fig. 4. A greater SAR reduction was clearly obtained with adapted rather than with stretched RF pulses. A quantitative comparison over the entire 3D SAR data is summarized in Fig. 5. Using adapted RF pulses effectively reduced SAR by as much as 70% at the cost of a slight increase in pulse duration, resulting in lower SAR levels than with stretched gradient for same pulse duration (Figs. 4 and 5). Even considering the slight increase in pulse duration, the RF pulses designed using adapted rate k-space trajectories for a reduction factor of 4 were still much shorter than those without reduction (~4 ms or less vs. 10.2 ms). Similar results were observed for both small (20°) and large (90°) tip angles, which was expected due to the linear properties of the chosen RF pulse design method.

Fig. 7 displays the original and adapted gradient waveforms and corresponding RF pulses used for experiments in a phantom with two different flip angles, using as excitation target the small off

centered smoothed circle shown in Fig. 8a. For both small (20°) and large (90°) nominal flip angles, adapting the gradient waveforms for RF pulse calculation substantially suppressed high peak values observed in original RF pulses. As shown in Fig. 8b and c, this experimental verification confirmed that excitation pattern accuracy was comparable for original and adapted RF pulses, closely matching the excitation target (Fig. 8a).

The critical impact of the third step in the proposed RF pulse design can be appreciated in Fig. 9 where adapted RF pulses obtained by direct manipulation of original RF pulse are compared with adapted RF pulses redesigned when ΔB_0 maps are included. Although direct manipulation of original pulses never violated the preset threshold, with RFSOM always lower or equal to threshold a (Fig. 9c), this approach, which cannot account for ΔB_0 maps (or any possible k-space deviations), resulted in significant errors in the excitation pattern (Fig. 9d, left). By comparison, redesigning adapted RF pulses *with* ΔB_0 correction provided satisfactory excitation fidelity (Fig. 9d, right), at the cost of not strictly enforcing RFSOM $\leqslant a$: indeed, RFSOM was sometimes larger than a. However, the latter case was observed only in a small fraction of the RF pulse duration and, in these cases, RFSOM exceeded a only by a small amount.

5. Discussion and conclusion

We have proposed and demonstrated at 9.4 T an RF pulse design method for effective SAR reduction in 2D parallel excitation based on the variable rate principle that had initially been described in VERSE for 1D selective excitation with a single transmit channel [23]. In the presented method, adapted RF pulses are calculated in three steps. First, an original RF pulse is designed with predefined fastest k-space trajectories. Adapted rate k-space trajectories are then calculated based on this reference. Finally, optimized RF pulses are re-calculated based on the adapted rate trajectories. Simulation results based on electromagnetic modeling showed that with this approach SAR was effectively reduced at the cost of a slight increase in pulse duration, with much greater efficiency than when simply stretching RF pulses and gradient waveform to the same final RF pulse duration. Experimental results obtained in a phantom at 9.4 T demonstrated that excitation patterns were not altered by these adapted low SAR RF pulses.

Compared with other methods previously proposed for reducing SAR in parallel excitation using gradient manipulation, our approach has several advantages. Unlike the k-space domain method [17], our gradient manipulations are directly based on calculated RF pulses without relying on the Fourier transform of the excitation patterns and hence can provide optimized pulses for arbitrary flip angles. Unlike the variable slew rate method [19], it adapts gradient amplitudes without requiring analytical gradient formulations and, therefore, can in principle apply to any type of gradient waveform. Unlike the time-optimal pulse design [20] where the final variable rate RF pulses are obtained by directly manipulating the original pulses, our method in the last step recalculates the adapted RF pulses by using the adapted gradient waveforms as the input to the selected parallel transmit pulse design algorithm. It has been shown that such recalculation is crucial in order to achieve satisfactory excitation accuracy at high field when main field nonuniformities and/or gradient imperfections have to be compensated.

In its current implementation our method also has a few limitations. First, it only includes decreases in gradient strengths, inevitably resulting in increased pulse duration. This is however a practical consequence of our current hardware configuration: with limited gradient strength and limited slew rate, we always have to start with the shortest possible original RF pulses, so k-space traversals can only be *slowed down* to not violate gradient slew rate limits. If original pulses (before adaptation) were not squeezed to their shortest possible duration, our final adapted RF pulses could be even further shortened by speeding up k-space traversals during segments of lower RF amplitude in the original pulse. Second, our method requires RF pulses to be calculated twice, which in principle doubles the RF computation time. However, considering the constant increase in calculation speed on computers, it seems reasonable to assume that this should not constitute a significant limitation.

Since the difference in SAR reduction obtained using adapted vs. stretched RF pulses tended to be somewhat smaller when using a small ellipse target (compared with larger targets), it could be questioned whether in this case this difference could be matched up by increasing the regularization parameter in the stretched pulse calculation (first group of methods, see Introduction). However, increasing the regularization parameter will inherently compromise excitation accuracy, thus only limited improvement would be expected in this case. This was verified in additional simulations showing that, even when using the small ellipse target, the regularization parameter had to be set to about twice the value indicated by the L-curve criterion, resulting in a drastic increase in excitation errors ($||\boldsymbol{Ab} - \boldsymbol{\theta}||/||\boldsymbol{\theta}||$, rose from 6% to 15%) with noticeable excitation artifacts.

In conclusion, we have introduced a 3-step adapted rate RF pulse design for effective SAR reduction in parallel transmission. Our simulation and experiment results for 8-channel 2D parallel transmission at 9.4 T show that adapted rate RF pulses are more efficient in reducing SAR than those generated by linearly stretching the original pulses. The third step of our methods consisting of redesigning the final adapted RF pulses based on adapted gradient waveform ensures that excitation fidelity is preserved.

Acknowledgments

The authors would like to acknowledge Lance DelaBarre for his help with setting up the 9.4 T multi-transmit system, Gregor Adriany and Carl Snyder for building the RF coils used in this study, Dinesh Deelchand and Pierre-Gilles Henry for their assistance with 3D AFI sequence development. We would also like to acknowledge the anonymous reviewers for their useful suggestions. This work was supported by the KECK Foundation and NIH funding (EB006835, EB007327, P41 RR008079 and P30 NS057091).

References

[1] U. Katscher, P. Bornert, C. Leussler, J.S. van den Brink, Transmit SENSE, Magn. Reson. Med. 49 (2003) 144–150.
[2] Y. Zhu, Parallel excitation with an array of transmit coils, Magn. Reson. Med. 51 (2004) 775–784.
[3] C.J. Hardy, H.E. Cline, Spatial localization in 2 dimensions using Nmr designer pulses, J. Magn. Reson. 82 (1989) 647–654.
[4] J. Pauly, D. Nishimura, A. Macovski, A k-space analysis of small-tip-angle excitation, J. Magn. Reson. 81 (1989) 43–56.
[5] K. Setsompop, V. Alagappan, B. Gagoski, T. Witzel, J. Polimeni, A. Potthast, F. Hebrank, U. Fontius, F. Schmitt, L.L. Wald, E. Adalsteinsson, Slice-selective RF pulses for in vivo B1+ inhomogeneity mitigation at 7 Tesla using parallel RF excitation with a 16-element coil, Magn. Reson. Med. 60 (2008) 1422–1432.
[6] Z. Zhang, C.Y. Yip, W. Grissom, D.C. Noll, F.E. Boada, V.A. Stenger, Reduction of transmitter B1 inhomogeneity with transmit SENSE slice-select pulses, Magn. Reson. Med. 57 (2007) 842–847.
[7] W. Grissom, C.Y. Yip, Z. Zhang, V.A. Stenger, J.A. Fessler, D.C. Noll, Spatial domain method for the design of RF pulses in multicoil parallel excitation, Magn. Reson. Med. 56 (2006) 620–629.
[8] K. Setsompop, L.L. Wald, V. Alagappan, B. Gagoski, F. Hebrank, U. Fontius, F. Schmitt, E. Adalsteinsson, Parallel RF transmission with eight channels at 3 Tesla, Magn. Reson. Med. 56 (2006) 1163–1171.
[9] P. Ullmann, S. Junge, M. Wick, F. Seifert, W. Ruhm, J. Hennig, Experimental analysis of parallel excitation using dedicated coil setups and simultaneous RF transmission on multiple channels, Magn. Reson. Med. 54 (2005) 994–1001.

[10] U. Katscher, P. Vernickel, J. Overweg, Basics of RF power behaviour in parallel transmission, in: Proceedings of the 13th Scientific Meeting of ISMRM, Miami, USA, 2005, p. 17.
[11] P. Ullmann, G. Wuebbeler, S. Junge, F. Seifert, W. Ruhm, J. Hennig, SAR-analysis for transmit SENSE with a 4-channel head array at 3 T, in: Proceedings of the 14th Scientific Meeting of ISMRM, Seattle, USA, 2006, p. 601.
[12] X. Wu, C. Akgun, J.T. Vaughan, K. Ugurbil, P.F. Van de Moortele, SAR analysis for transmit SENSE at 7 T with a human head model, in: Proceedings of the 15th Scientific Meeting of ISMRM, Berlin, Germany, 2007, p. 3350.
[13] J.T. Vaughan, M. Garwood, C.M. Collins, W. Liu, L. DelaBarre, G. Adriany, P. Andersen, H. Merkle, R. Goebel, M.B. Smith, K. Ugurbil, 7 T vs. 4 T: RF power, homogeneity, and signal-to-noise comparison in head images, Magn. Reson. Med. 46 (2001) 24–30.
[14] A.C. Zelinski, K. Setsompop, V. Alagappan, B.A. Gagoski, L.M. Angelone, G. Bonmassar, U. Fontius, F. Schmitt, E. Adalsteinsson, L.L. Wald, Pulse design methods for reduction of specific absorption rate in parallel RF excitation, in: Proceedings of the 15th Scientific Meeting of ISMRM, Berlin, Germany, 2007, p. 1698.
[15] R. Lattanzi, D.K. Sodickson, A.K. Grant, Y. Zhu, Electrodynamic constraints on homogeneity and radiofrequency power deposition in multiple coil excitations, Magn. Reson. Med. 61 (2009) 315–334.
[16] I. Graesslin, J. Weller, F. Schweser, B. Annighoefer, S. Biederer, U. Katscher, T. Nielsen, P. Harvey, P. Börnert, SAR hotspot reduction by temporal averaging in parallel transmission, in: Proceedings of the 17th Scientific Meeting of ISMRM, Honolulu, USA, 2009, p. 176.
[17] I. Graesslin, S. Biederer, F. Schweser, K.H. Zimmermann, U. Katscher, P. Börnert, SAR reduction for parallel transmission using VERSE and k-space filtering, in: Proceedings of the 15th Scientific Meeting of ISMRM, Berlin, Germany, 2007, p. 674.
[18] J. Pauly, D. Nishimura, A. Macovski, A linear class of large-tip-angle selective excitation pulses, J. Magn. Reson. 82 (1989) 571–587.
[19] D. Xu, K.F. King, Z.P. Liang, Variable slew-rate spiral design: theory and application to peak B(1) amplitude reduction in 2D RF pulse design, Magn. Reson. Med. 58 (2007) 835–842.
[20] D. Lee, M. Lustig, W.A. Grissom, J.M. Pauly, Time-optimal design for multidimensional and parallel transmit variable-rate selective excitation, Magn. Reson. Med. 61 (2009) 1471–1479.
[21] X. Wu, C. Akgun, J.T. Vaughan, K. Ugurbil, P.F. Van de Moortele, SAR reduction in transmit SENSE using adapted excitation k-space trajectories, in: Proceedings of the 15th Scientific Meeting of ISMRM, Berlin, Germany, 2007, p. 673.
[22] X. Wu, J.T. Vaughan, K. Ugurbil, P.F. Van de Moortele, Parallel excitation in the human brain at 9.4 T counteracting k-space errors with RF pulse design, Magn. Reson. Med. 63 (2010) 524–529.
[23] S. Conolly, D. Nishimura, A. Macovski, G. Glover, Variable-rate selective excitation, J. Magn. Reson. 78 (1988) 440–458.
[24] X. Wu, J. Vaughan, K. Ugurbil, P. Van de Moortele, Implementation of VERSE parallel transmission at 9.4 T, in: Proceedings of the 17th Scientific Meeting of ISMRM, Honolulu, USA, 2009, p. 2591.
[25] P.A. Bottomley, E.R. Andrew, RF magnetic field penetration, phase shift and power dissipation in biological tissue: implications for NMR imaging, Phys. Med. Biol. 23 (1978) 630–643.
[26] C.M. Collins, S. Li, M.B. Smith, SAR and B1 field distributions in a heterogeneous human head model within a birdcage coil. Specific energy absorption rate, Magn. Reson. Med. 40 (1998) 847–856.
[27] D.I. Hoult, D. Phil, Sensitivity and power deposition in a high-field imaging experiment, J. Magn. Reson. Imaging 12 (2000) 46–67.
[28] U. Katscher, J. Rohrs, P. Bornert, Basic considerations on the impact of the coil array on the performance of Transmit SENSE, Magma (New York, NY) 18 (2005) 81–88.
[29] G. Adriany, P.F. Van de Moortele, F. Wiesinger, P. Andersen, J.P. Strupp, X. Zhang, C. Snyder, W. Chen, K.P. Pruessmann, P. Boesiger, J.T. Vaughan, K. Ugurbil, Transceive stripline arrays for ultra high field parallel imaging applications, in: Proceedings of the 11th Scientific Meeting of ISMRM, Toronto, Canada, 2003, p. 474.
[30] D. Xu, K.F. King, Y. Zhu, G.C. McKinnon, Z.P. Liang, A noniterative method to design large-tip-angle multidimensional spatially-selective radio frequency pulses for parallel transmission, Magn. Reson. Med. 58 (2007) 326–334.
[31] G. Adriany, P.F. Van de Moortele, F. Wiesinger, S. Moeller, J.P. Strupp, P. Andersen, C. Snyder, X. Zhang, W. Chen, K.P. Pruessmann, P. Boesiger, T. Vaughan, K. Ugurbil, Transmit and receive transmission line arrays for 7 Tesla parallel imaging, Magn. Reson. Med. 53 (2005) 434–445.
[32] G.H. Glover, Simple analytic spiral k-space algorithm, Magn. Reson. Med. 42 (1999) 412–415.
[33] V.L. Yarnykh, Actual flip-angle imaging in the pulsed steady state: a method for rapid three-dimensional mapping of the transmitted radiofrequency field, Magn. Reson. Med. 57 (2007) 192–200.
[34] P.F. Van de Moortele, C. Snyder, L. DelaBarre, C. Akgun, X. Wu, T. Vaughan, K. Ugurbil, Fast Mapping of Relative B1+ Phase in the Human Head at 9.4 Tesla with a 14 Channel Transceive Coil Array, Intnl Symposium on Biomed Magn Reson Imaging and Spectroscopy at Very High Fields, Wuerzburg, 2006, p. 37.
[35] G. Metzger, C. Snyder, C. Akgun, T. Vaughan, K. Ugurbil, P.F. Van de Moortele, Local B1+ shimming for prostate imaging with transceiver arrays at 7 Tesla based on subject dependent transmit phase measurements, Magn. Reson. Med. 59 (2008) 396–409.
[36] P.F. Van de Moortele, C. Akgun, G. Adriany, S. Moeller, J. Ritter, C.M. Collins, M.B. Smith, J.T. Vaughan, K. Ugurbil, B1 destructive interferences and spatial phase patterns at 7 T with a head transceiver array coil, Magn. Reson. Med. 54 (2005) 1503–1518.
[37] J.H. Duyn, Y. Yang, J.A. Frank, J.W. van der Veen, Simple correction method for k-space trajectory deviations in MRI, J. Magn. Reson. 132 (1998) 150–153.